Supplementary material

A. Experimental setup

The full measurement setup is shown in Fig. S1. The device was placed in a dilution refrigerator at a base temperature of 20 mK, and the transmission measurements were performed using a Vector Network Analyzer (VNA). An additional microwave source was used for two-tone measurements, while a global magnetic field was applied via an external superconducting coil. Both the coil and the sample were held inside a mu-metal magnetic shield which is coated on the inside with a light absorber made out of epoxy loaded with silicon and carbon powder. The output line included two isolators at 20 mK, a HEMT amplifier at 4 K and a room temperature amplifier. The input line is attenuated at various stages, including a home-made filter that prevents stray-radiations from reaching the sample. We adopted a coaxial geometry with a dissipative dielectric (reference RS-4050 from resin systems company). The bandwidth of the measurement setup goes from 2.5 GHz to 13 GHz.

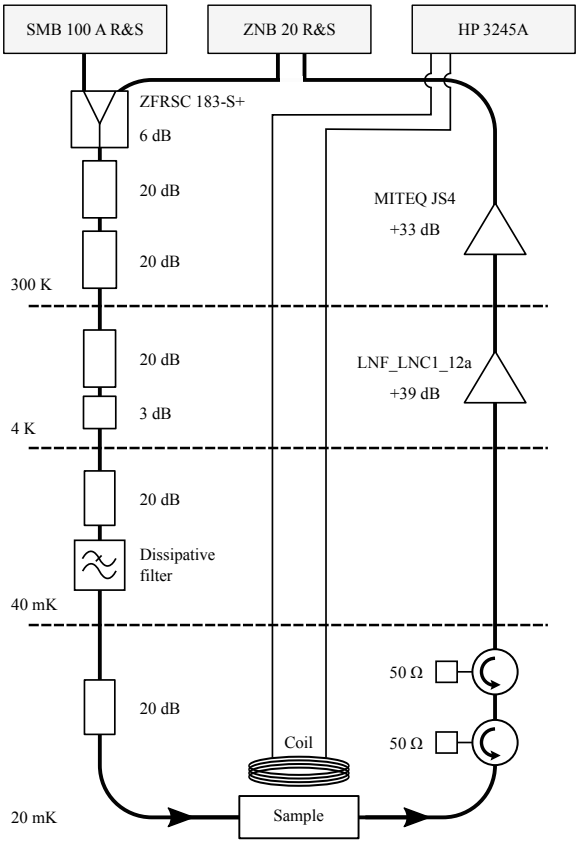

FIG. S1. **Experimental setup.**

B. Chain dispersion relation

In this section we explain how we experimentally obtained the dispersion relation of the chain, and how we used it to determine the model parameters $L_{J,\min}$, C_{g} and C_J that characterize the chain. (See *Methods - Sample fabrication and parameters* in the main text.) The experimental data in Fig. S2**a** (reproduced from Fig. 2**b** in main text) was obtained by first tuning the external magnetic field to a point where $\Phi_{\mathrm{T}} = \Phi_0/2$ so that $E_{J,\mathrm{T}}(\Phi_{\mathrm{T}}) = 0$. (Green dashed line in the inset to Fig. S2**a**.) This leads to vanishingly low transmon frequency. As a result, the transmon does not contribute any degrees of freedom that can hybridize with the bare modes of the chain. In order to realize a good fit, one needs

to measure the spectrum in a wide frequency band (0.1 GHz to 20 GHz). One is however limited by the bandwidth of the setup (2.5 GHz to 13 GHz). This difficulty can be overcome by performing a two-tone measurement[1–3], taking advantage of the fact that the array is not perfectly linear. As a consequence, when applying a microwave tone at a given resonance of the chain, the other resonant frequencies are shifted by the cross Kerr effect. With the Vector Network Analyzer (VNA), we proceed by measuring the transmission of the system at a fixed frequency $\omega_{\mathrm{VNA}} = \omega_1$ where ω_1 matches a given resonance frequency of the circuit. Then with a microwave source we apply a second tone at a variable frequency ω_{MW}. Whenever ω_{MW} equals any other resonance frequency of the circuit, ω_1 shifts to $\tilde{\omega}_1$ due to the cross Kerr effect, so that $\omega_{\mathrm{VNA}} \neq \tilde{\omega}_1$, which leads to a dip in transmission. The value of ω_{MW} at these dips provides all the resonances of the system. Because we measure at a constant frequency ω_{VNA} inside the setup bandwidth, we are not limited by the frequency range of our measurement setup anymore. A typical two-tone measurement is shown in Fig. S2**b**, where we fit each dip separately with a Lorentzian. The center frequencies obtained from these fits are the experimental points in Fig. S2**a** for the eigenmodes of the chain.

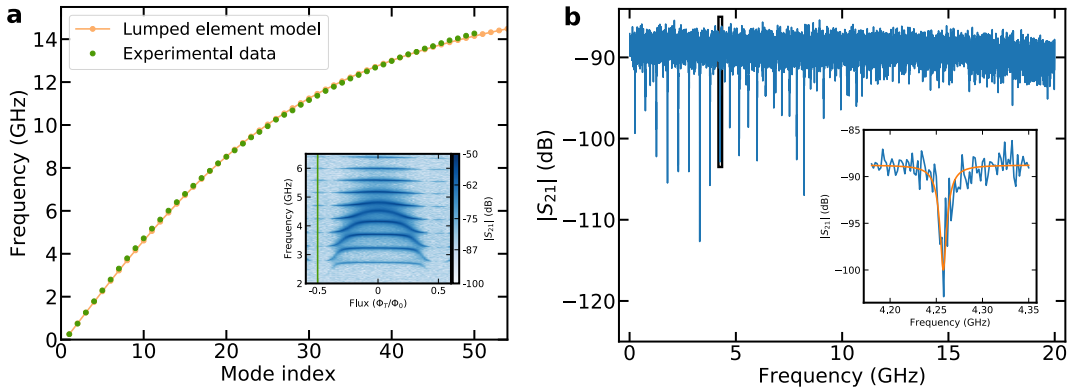

FIG. S2. **Extraction of the individual chain modes. a** Dispersion relation of the chain, reproduced from Fig. 2**b** in main text. The inset shows a colourscale plot of the transmission amplitude as function of Φ_{T} and probe frequency, with a green line indicating the fixed flux value employed to determine the dispersion relation of the uncoupled chain. **b** Two tone measurement of the modes of the array. The frequency trace is along the green line in panel *a*. The inset shows a lorentzian fit of one of the dips. The measurement was taken with $P_{\mathrm{VNA}} = -10\,\mathrm{dBm}$ and $P_{\mathrm{MW}} = 10\,\mathrm{dBm}$ at room temperature. The frequency of the VNA was set to $\omega_{\mathrm{VNA}} = 5.1692\,\mathrm{GHz}$.

In order to fit the experimental data for the chain modes, we assume that the left end of the chain is open when $\Phi_{\mathrm{T}} = 0.5\ \Phi_0$ ($E_{J,\mathrm{T}} = 0$). We also take the right end of the chain to be grounded. Given that the chain SQUIDS are designed to have a Josephson energy several thousand times their charging energy ($E_J/E_C = 8400$), we can model the Josephson junctions in the chain as linear inductors with inductance $L_J(\Phi_{\mathrm{C}}) = \varphi_0^2/E_J(\Phi_{\mathrm{C}})$, with $\varphi_0 = \hbar/2e$ the reduced flux quantum. The theoretical dispersion relation can be obtained applying Kirchoff's laws to one chain cell of length a. (See the circuit diagram in Fig. 1**a** in the main text.) Denoting the flux at node j as Φ_j, we obtain

$$\frac{1}{L_J(\Phi_{\mathrm{C}})}\left(\Phi_{j-1}-\Phi_j\right) + C_J\left(\ddot{\Phi}_{j-1}-\ddot{\Phi}_j\right) - \frac{1}{L_J(\Phi_{\mathrm{C}})}\left(\Phi_j-\Phi_{j+1}\right) - C_J\left(\ddot{\Phi}_j-\ddot{\Phi}_{j+1}\right) - C_{\mathrm{g}}\ddot{\Phi}_j = 0. \tag{S1}$$

Now if we use as ansatz a plane waves $\Phi_j = A\exp i\left(\omega t - \kappa j a\right) + B\exp i\left(-\omega t + \kappa j a\right)$ and solve for ω we obtain the dispersion relation for a bare chain

$$\omega\left(\kappa\right) = \frac{1}{\sqrt{L_J(\Phi_{\mathrm{C}})C_J}}\sqrt{\frac{1-\cos\left(\kappa a\right)}{1-\cos\left(\kappa a\right)+\frac{C_{\mathrm{g}}}{2C_J}}}. \tag{S2}$$

The boundary conditions at site 0 (vacuum) and at site N (grounded) read

$$\left.\frac{\partial\Phi_j}{\partial(ja)}\right|_{j=0} = 0, \tag{S3}$$

$$\dot{\Phi}(N) = 0, \tag{S4}$$

which restricts the values of κa to

$$\kappa a = \frac{\left(n-\frac{1}{2}\right)\pi}{N} \qquad n = 1, 2, \ldots, N. \tag{S5}$$

Since the areas of chain SQUID loops are much smaller than that of the transmon SQUID loop, at $\Phi_T = \Phi_0/2$ we can tune the flux Φ_C through each chain SQUID to a multiple of Φ_0, so that the chain SQUID inductance is minimal, i.e. $L_J(\Phi_C) = L_{J,\min}$, without appreciably changing the transmon flux Φ_T from its value $\Phi_0/2$. (See Eq. (3) in the *Methods* section of the main text.) Using Eq. (S2) with the κ values from Eq. (S5), we fit the experimental data in Fig. S2**a** (orange curve), thus fixing the minimal Josephson inductance $L_{J,\min}$ and the capacitance to ground C_g. We obtain the Josephson self-capacitance C_J using the empirical formula[4]

$$C_J = 45\,\mathrm{fF}/\mu\mathrm{m}^2 \times \text{junction area}. \tag{S6}$$

The error for C_J is just the error we obtain for the measurement of the Josephson junction's area using a Scanning Electron Microscope. The error for $L_{J,\min}$ and C_g are the values where the deviation between the experiment and the fit was below 5 %.

C. Additional phase shift data

In this section we present a further selection of relative phase shift data $\delta\phi_n$ obtained for various (Φ_T,Φ_C) combination. This is only a small subset of the full data set, and the agreement between theory and experiment exhibited here is representative of the full data set. Results presented here complement Fig. 4**a** of the main text. The parameters used to obtain the theory curves are the ones of Table S1.

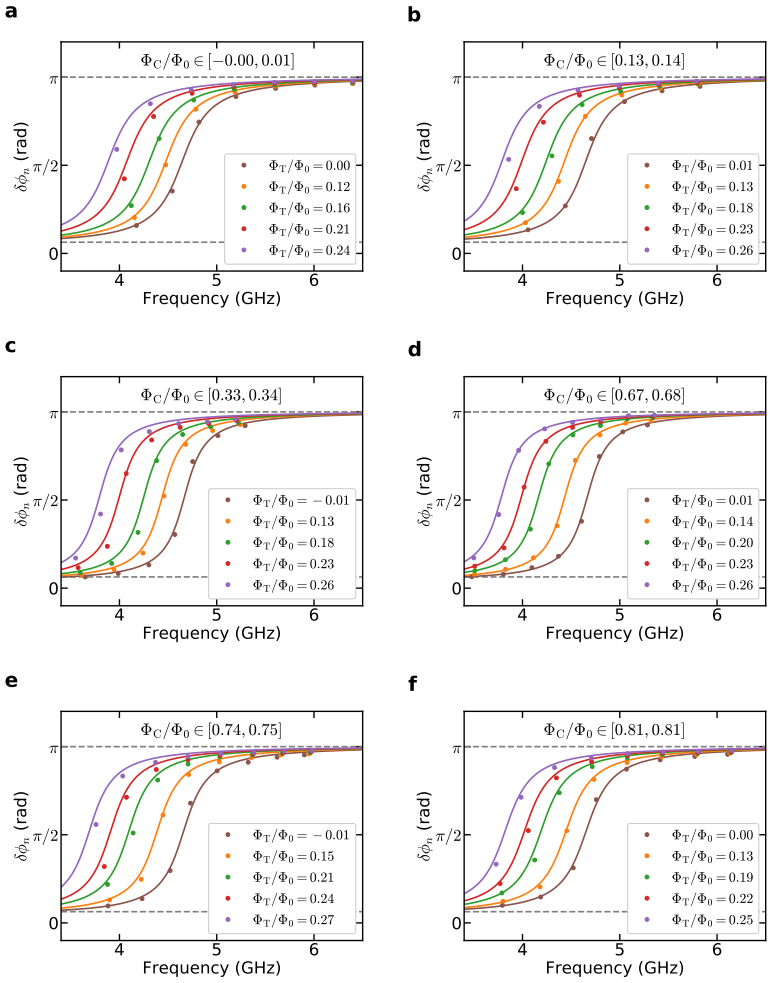

FIG. S3. **Consistency of the theoretical model for several transmon and chain fluxes.** The various panels show the relative phase shift $\delta\phi_n$ of the discrete chain modes as a function of mode frequency ω_n for different transmon fluxes Φ_T and chain fluxes Φ_C. The solid lines are fits using Eq. (14) of the main text with the parameters of the circuit kept fixed.

D. Transmon qubit capacitances estimation

In order to obtain the capacitances listed in Table S1 (reproduced from the main text) we use EM simulation software (Sonnet). This software solves Maxwell's equations in three dimensions for the specified design of our device and gives the scattering parameters of the system as a function of frequency. We simulate two parts of the design independently, the interdigital capacitors and the SQUID of the transmon qubit.

Chain parameters	
$L_{J,\min}$	(0.33 ± 0.02) nH
C_g	(0.13 ± 0.01) fF
C_J	(259 ± 14) fF
N	4700
d (asymmetry)	0.25

Transmon qubit parameters	
$C_{g,T2}$	(33 ± 1) fF
$C_{g,T}$	(48 ± 2) fF
C_c	(119 ± 2) fF
C_{sh}	(6.9 ± 0.1) fF
$C_{J,T}$	(5.2 ± 0.3) fF
$E_{J,T,\max}/h$	(10.2 ± 0.4) GHz
$E_{C,T}/h$	(2.4 ± 0.1) GHz

TABLE S1. **Sample parameters.**

1. *Interdigital capacitors*

Since we are only interested in modelling the capacitors of the transmon, we remove the chain from the simulation and replace the Josephson junction of the transmon by a linear inductor, L_{test}. We place two ports at both ends of the design, and set the characteristic impedance of the port on the left to Z_{left} and for the port on the right to Z_{right}.

From the EM simulation we obtain the transmission of the system, S_{21}, as a function of frequency. We fit the prediction of the linear model of the qubit to this. This model consists of the capacitance network shown in Fig. S4 in red. The transmission of this system is given by Eq. (S7)[5] where A, B, C and D are the ABCD matrix elements[6]

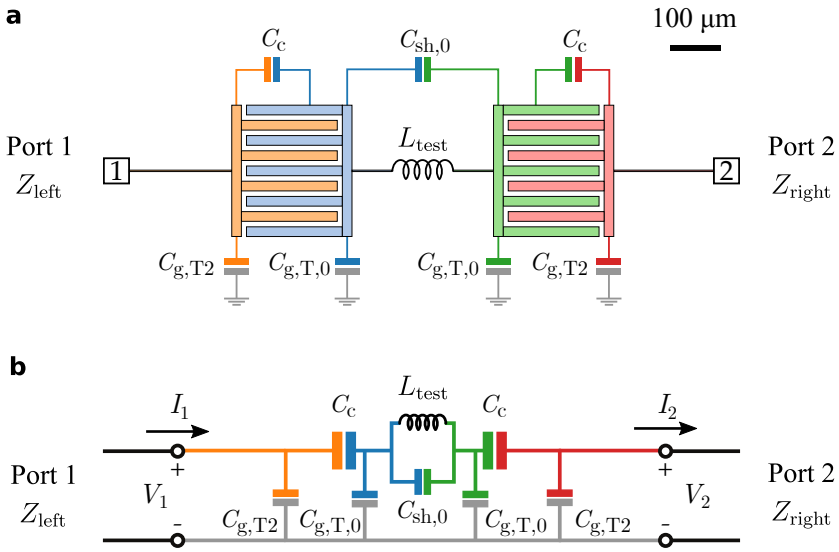

FIG. S4. **Model for the linear transmon coupling. a** Real capacitor design.**b** Lumped element model used in the EM simulations.

for the capacitance network plus the linear inductor.

$$S_{21} = \frac{2\sqrt{Z_{\text{left}} Z_{\text{right}}}}{AZ_{\text{right}} + B + CZ_{\text{left}} Z_{\text{right}} + DZ_{\text{left}}}. \tag{S7}$$

In theory L_{test}, Z_{left}, Z_{right} do not affect the obtained capacitances and can be chosen arbitrarily. However, due to the fact that the lumped element model is an idealization, we observed a small shift of the capacitances as a function of L_{test}. (This shift was not observed as a function of Z_{left} or Z_{right}). To minimize the effect of this shift, we set $L_{\text{test}} = 22\,\text{nH}$ which gives a resonance frequency close to ω_T.

We perform two simulations. In the first one we set $Z_{\text{left}} = Z_{\text{right}} = 50\,\Omega$. Due to the low impedance of the ports, we can neglect $C_{\text{g,T2}}$ and we therefore fit only C_{c}, $C_{\text{g,T,0}}$ and $C_{\text{sh,0}}$. Then we perform a second simulation with $Z_{\text{left}} = 50\,\Omega$ and $Z_{\text{right}} = 3000\,\Omega$. Now we fit only $C_{\text{g,T2}}$ keeping the other capacitances constant. In this way we obtain all the capacitances in Fig. S4 independently. Note that the self-capacitance of the junction $C_{J,\text{T}}$ cannot be simulated and is therefore obtained from Eq. (S6). The errors are obtained as the maximum range where the difference between simulation and model is smaller than 10 %. The two fits are shown in Fig. S5.

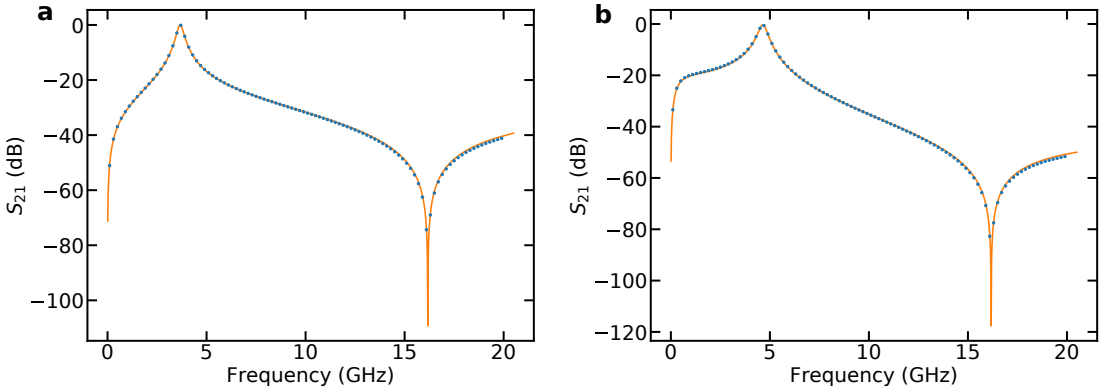

FIG. S5. **Extraction of the coupling capacitances.** Fit of the obtained S_{21} parameter to a linear model with $Z_{\text{right}} = 50\,\Omega$ (left panel **a**) and $Z_{\text{right}} = 3000\,\Omega$ (right panel **b**).

2. *Stray capacitances from the transmon SQUID*

The transmon qubit has a SQUID with a large loop ($\sim 55\,\mu\text{m} \times 1.2\,\mu\text{m}$). Due to its large size, the capacitances associated to this SQUID are not negligible. In Fig. S6**a** the SQUID design with the different capacitances is given. The lumped element model used for simulating the system is shown in Fig. S6**b**.

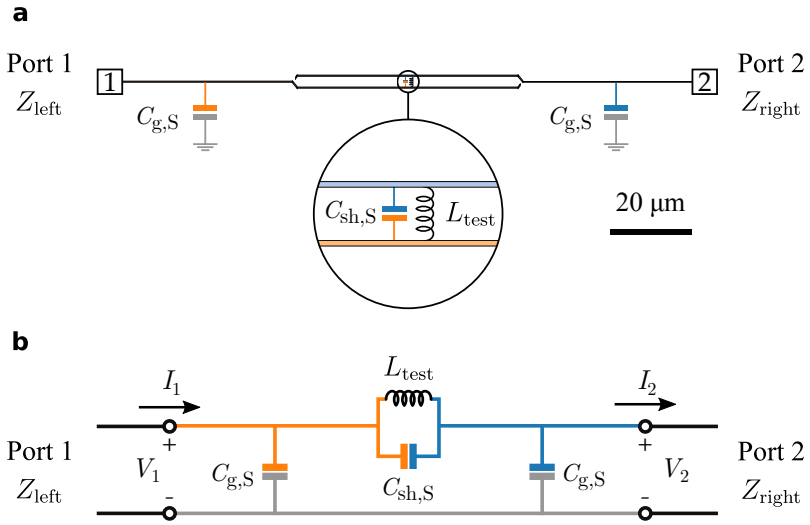

FIG. S6. **Internal capacitance model for the transmon. a** Real design of the SQUID of the transmon qubit. In the inset the shunting capacitance $C_{\text{sh,S}}$ and test inductance L_{test} are shown. **b** Lumped element model used to simulate the capacitances of the system.

We follow the same procedure as before. Given the small number of fitting parameters ($C_{\text{sh,S}}$ and $C_{\text{g,S}}$) we can perform a single fit with $Z_{\text{left}} = 50\,\Omega$ and $Z_{\text{right}} = 3000\,\Omega$. The result of the fit is shown in Fig. S7 with the obtained capacitance values. The SQUID increases both the shunting capacitance and the ground capacitance of the transmon qubit.

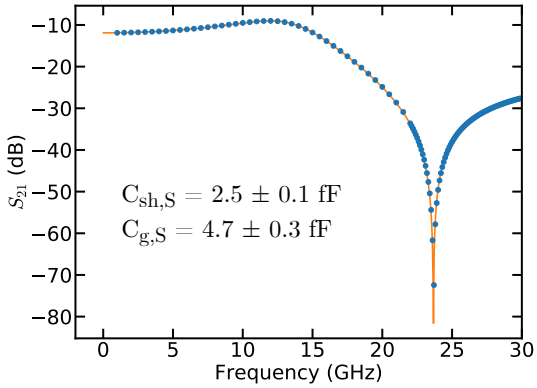

FIG. S7. **Extraction of the internal capacitances.** SQUID capacitances estimation. Simulated transmission (blue circles) and fit from the lumped element model, orange solid line. The simulation was performed setting $Z_{\text{left}} = 50\,\Omega$ and $Z_{\text{right}} = 3000\,\Omega$.

E. How does the transmon decay rate depends on the impedance of the environment?

Before quantitatively modeling the system, in this section we try to gain a qualitative understanding of how the transmon decay rate Γ_{T} depends on the characteristic impedance of the chain. Since we are only aiming for a qualitative description, we treat the transmon SQUID loop as an LC circuit, ignoring its non-linearity. We retain the capacitive couplings C_{c}, that couple the transmon to the chain and the 50 Ω transmission line. We drop the ground capacitances $C_{\text{g,T}}$ and $C_{\text{g,T2}}$ that shunt the chain at high frequencies, thus idealizing to the situation where the chain produces an optimal broadening of the transmon resonance. We consider an infinite chain. Since we are not interested here in modeling frequency dependent transport through the system, but only in the effect the chain has on the transmon, we replace the complicated frequency dependent impedance of the chain $Z_{\text{chain}}(\omega)$ with its constant characteristic impedance $R = \sqrt{L_J/C_{\text{g}}}$. We replace the 50 Ω (low impedance) transmission lines by ground connections. These assumptions produce the simple linear circuit depicted in Fig. S8.

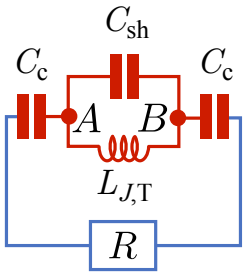

FIG. S8. **Toy model of the whole circuit.** Simplified lumped element model used to qualitatively understand the link between the transmon decay rate and the impedance of the environment.

Within this linear model, the resonance frequency ω_{T} and decay rate Γ_{T} of the transmon are obtained as respectively the real and imaginary parts of the relevant pole of the frequency dependent impedance between A and B in the circuit diagram. This impedance is given by

$$Z_{AB}(\omega) = \frac{iL_{J,\text{T}}\omega(2 + iC_{\text{c}}R\omega)}{(2 + iRC_{\text{c}}\omega)(1 - L_{J,\text{T}}C_{\text{sh}}\omega^2) - L_{J,\text{T}}C_{\text{c}}\omega^2} \tag{S8}$$

We have to note here that we have oversimplified the model, which now predicts an overdamped regime at small C_{sh}. In the real device, overdamping is prevented by the sizable capacitances $C_{\text{g,T}}$ and $C_{\text{g,T2}}$, which we have dropped. A quick fix, is to use a value for C_{sh} that is comparable to $C_{\text{g,T}}$ and $C_{\text{g,T2}}$ (several tens of fF), rather than its actual value of 4.4 fF. The behavior of the resonance frequency is easy to understand. At small R, one effectively has an LC circuit with capacitance $C_{\text{sh}} + C_{\text{c}}/2$ and resonance frequency $\omega_{\text{T}} = 1/\sqrt{L_{J,\text{T}}(C_{\text{sh}} + C_{\text{c}}/2)}$, while at large R, one has an isolated SQUID loop with resonance frequency $\omega_{\text{T}} = 1/\sqrt{L_{J,\text{T}}C_{\text{sh}}}$.

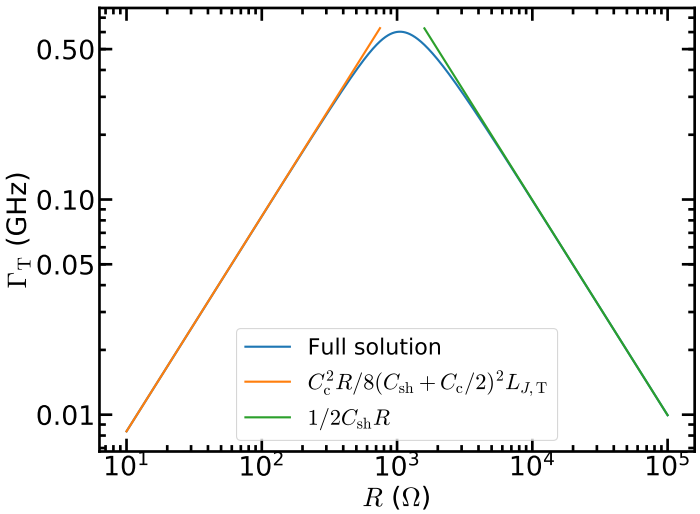

FIG. S9. **Bath engineered dissipation from the toy model.** Evolution of the transmon decay rate Γ_T versus the value of the resistance R, as described in the simplified circuit of Fig. S8.

In Fig. S9 we present the behavior of Γ_T vs. R for $C_c = 119$ fF (its actual value) and $C_{sh} = 80$ fF, chosen to give rough quantitative agreement with the experimental results we present in the Fig. 4 of the main text, although the qualitative behavior does not change if we change C_{sh} moderately. At small R, the behavior of the decay rate Γ_T is

$$\Gamma_T = \frac{C_c^2 R}{8(C_{sh}+C_c/2)^2 L_{J,T}} \tag{S9}$$

(proportional to R) while at large R, it is given by

$$\Gamma_T = \frac{1}{2C_{sh}R} \tag{S10}$$

(proportional to $1/R$). A good estimate of the value R_* that maximizes Γ_T is obtained by equating the small and large R asymptotic expressions for Γ_T. This yields

$$R_* = \left(1+\frac{2C_{sh}}{C_c}\right) Z_{T,simp} \tag{S11}$$

where $Z_{T,simp} = \sqrt{L_{J,T}/C_{sh}}$ is the characteristic impedance of the transmon, in the simplified circuit of Fig. S8. Thus the largest coupling (as measured by Γ_T) is obtained when the characteristic impedances of the transmon and chain match up to factors of order one, a result that is familiar in microwave engineering. At this optimal chain impedance, the decay rate Γ_T is proportional to ω_T with a proportionality constant that is a function of C_c/C_{sh}. This constant can reach values of order one, implying ultra-strong coupling is attainable. In our actual device, we find Γ_T to be a decreasing function of L_J, in the L_J window to which we have access, suggesting that the lowest chain impedance that we can reach, is larger than the optimal value R_*. When we compare the characteristic impedances $Z_T = \hbar/(2e)^2\sqrt{2E_{C,T}/E_{J,T}} \simeq 760\,\Omega$ (transmon) and $Z_C = \sqrt{L_J/C_g} \simeq 1590\,\Omega$ (chain) of the actual device, we see that indeed $Z_C > Z_T$. Note that here we took a realistic estimate for the transmon impedance, that includes the effect of the capacitances $C_{g,T}$ and $C_{g,T2}$ which were dropped in our qualitative model. Had we naively taken $Z_T = \sqrt{L_{J,T}/C_{sh}}$ we would have obtained $Z_T = 1990\ \Omega$, which though still close to the chain impedance, might have lead us to expect to observe a maximal value for Γ_T as we sweep the L_J window to which we have access.

F. Dealing with the transmon nonlinearity

The results in Fig. 3 in the main text confirm that the transmon qubit is a non-linear quantum circuit element that is strongly coupled to the chain. Here we review a standard way to deal with this anharmonicity.[7] The method is

known as the self-consistent harmonic approximation (SCHA) because the anharmonic term is replaced by a harmonic one whose magnitude is determined self-consistently, via the variational principle. We also determine the regime of validity of the approximations we introduce. Let us consider the complete Hamiltonian of the device, neglecting only the weak non-linearity in the chain elements:

$$H = \frac{E_{C,\mathrm{T}}}{2}\,\widehat{\mathrm{n}}_{\mathrm{T}}^2 - E_{J,\mathrm{T}}\cos(\widehat{\varphi}_{\mathrm{T}}) + \frac{(2e)^2}{2}\sum_{jl=1}^{N}\widehat{\mathrm{n}}_j\left[\widehat{\mathrm{C}}^{-1}\right]_{j,l}\widehat{\mathrm{n}}_l + \frac{E_J}{2}\sum_{j=1}^{N}\left(\widehat{\varphi}_{j+1}-\widehat{\varphi}_j\right)^2 + \widehat{\mathrm{n}}_{\mathrm{T}}\sum_{j=1}^{N}\nu_j\,\widehat{\mathrm{n}}_j\,. \tag{S12}$$

Here we found it convenient to define an operator $\widehat{\varphi}_{N+1} \equiv 0$ which is not an extra degree of freedom, but simply the zero operator. To shorten notation we don't indicate the Φ_{T} dependence of $E_{J,\mathrm{T}}$ or the Φ_{C} dependence of E_J explicitly here. Were it not for the term $-E_{J,\mathrm{T}}\cos(\widehat{\varphi}_{\mathrm{T}})$, the quantum system described by the Hamiltonian in Eq. (S12) (Eq. 8 in the main text) would have been equivalent to a set of coupled harmonic oscillators, and therefore straightforward to solve. The term $-E_{J,\mathrm{T}}\cos(\widehat{\varphi}_{\mathrm{T}})$, not being quadratic in $\widehat{\varphi}_{\mathrm{T}}$, produces an interacting many-body problem. The strategy will be to replace the transmon terms in H with more tractable, yet accurate counterparts. For this purpose our starting point is to consider the Hamiltonian H in the limit where the inductances L_J between chain nodes go to infinity ($E_J \to 0$), so that the charge on each chain island is conserved, and we can treat $\widehat{\mathrm{n}}_j$, $j \in \{1;\,\ldots;\,N\}$ as ordinary numbers. Since the transmon then does not couple to any dynamical degrees of freedom, we refer it as isolated. The conserved chain charges contribute to the offset charge for $\widehat{\mathrm{n}}_{\mathrm{T}}$. We will abuse notation slightly and still denote the transmon's charge degree of freedom, which now incorporates this additional offset, by $\widehat{\mathrm{n}}_{\mathrm{T}}$. The isolated transmon Hamiltonian, in which reference to the conserved charges $\widehat{\mathrm{n}}_\alpha$, $\alpha \in \{1;\,\ldots;\,N\}$ has been eliminated, reads

$$H_{\mathrm{T}} = \frac{E_{C,\mathrm{T}}}{2}\,\widehat{\mathrm{n}}_{\mathrm{T}}^2 + E_{J,\mathrm{T}}[1-\cos(\widehat{\varphi}_{\mathrm{T}})]. \tag{S13}$$

Due to charge being quantized in units of $2e$, the state space of H_{T} is restricted to states $|\psi\rangle$ for which

$$e^{i2\pi\,\widehat{\mathrm{n}}_{\mathrm{T}}}\,|\psi\rangle = e^{-i2\pi n_{\mathrm{T}}}\,|\psi\rangle\,, \tag{S14}$$

where the offset charge n_{T} (an ordinary number) contains contributions from the total transmon charge, the charge on each chain island, and from gate charges. We denote the eigenbasis of $\widehat{\mathrm{n}}_{\mathrm{T}}$ by $|\nu\rangle$, i.e.

$$\widehat{\mathrm{n}}_{\mathrm{T}}\,|\nu\rangle = \nu\,|\nu\rangle\,. \tag{S15}$$

Owing to (S14), ν is quantized such that

$$\nu + n_{\mathrm{T}} \in \mathbb{Z}. \tag{S16}$$

The matrix elements of H_{T} in the $|\nu\rangle$ basis read

$$\langle\nu|\,H_{\mathrm{T}}\,|\nu'\rangle = \frac{E_{C,\mathrm{T}}\nu^2}{2}\delta_{\nu,\nu'} + \frac{E_{J,\mathrm{T}}}{2}\left(\delta_{\nu,\nu'+1}+\delta_{\nu,\nu'-1}\right). \tag{S17}$$

The problem is equivalent to that of a charge e particle of mass $E_{C,\mathrm{T}}^{-1}$ confined to a ring of circumference 2π that is threaded by a flux of n_{T} times the flux quantum $\Phi_0 = h/2e$. The phase observable $\widehat{\varphi}_{\mathrm{T}}$ plays the role of the position coordinate, and the particle has an electrostatic potential energy $E_{J,\mathrm{T}}(1-\cos\widehat{\varphi}_{\mathrm{T}})$. This system is easily solved numerically. In Figure S10 the low energy spectrum is plotted as a function of the offset charge n_{T}, for three $E_{C,\mathrm{T}}/E_{J,\mathrm{T}}$ ratios. States with energies sufficiently less than the height $2E_{J,\mathrm{T}}$ of the cosine well are insensitive to the offset charge n_{T}. This is easy to understand in the equivalent picture of the particle confined to a ring: Sensitivity to the flux inside the ring requires the interference of paths with different winding numbers around the ring. However, at energies below $2E_{J,\mathrm{T}}$, paths with non-zero winding number are exponentially suppressed by the tunneling amplitude to go through the cosine barrier. States with energy $\gtrsim 2E_{J,\mathrm{T}}$ on the other hand are sensitive to the offset charge n_{T}. As n_{T} varies form 0 to 1/2 (half a Cooper pair), each of these energies sweep through an interval (or band) of width comparable to the spacing between levels. In the equivalent picture of a particle on a ring, this is a manifestation of the Aharonov Bohm effect. In a real experiment, the offset charge n_{T} is subject to environmental noise. Performing spectroscopy on the levels sensitive to n_{T} will therefore produce a noisy signal in which the extracted level energy "jumps around" inside the band through which the energy sweeps as n_{T} is varied.

When we reduce L_J from infinity to its actual value, thus coupling the transmon to dynamical degrees of freedom in the chain, a numerically exact solution is no longer possible, given the large size of the Hilbert space. An obvious approximation scheme for states with energies below $2E_{J,\mathrm{T}}$ is the following. For these states, the phase observable $\widehat{\varphi}_{\mathrm{T}}$ is unlikely to make excursions over the top of the cosine barrier (phase slips) at $\varphi_{\mathrm{T}} = \pm\pi$. For such states it

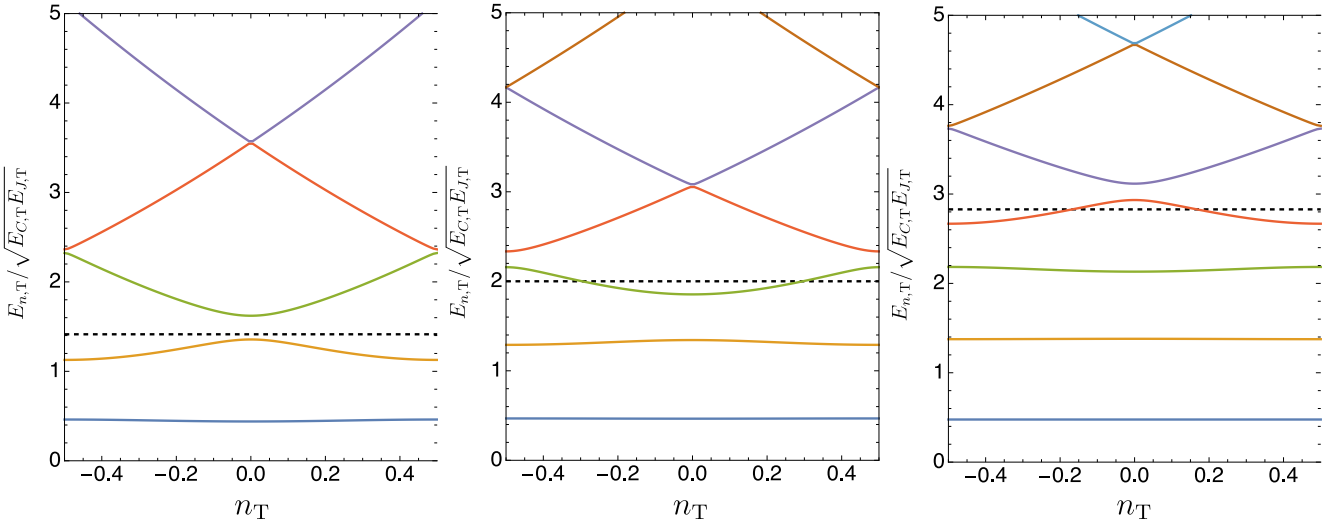

FIG. S10. **Isolated transmon spectrum as a function on the offset charge $\mathbf{n}_{\mathrm{T}}$.** Left panel: $E_{J,\mathrm{T}}/E_{C,\mathrm{T}} = 1/2$. Middle panel: $E_{J,\mathrm{T}}/E_{C,\mathrm{T}} = 1$. Right panel: $E_{J,\mathrm{T}}/E_{C,\mathrm{T}} = 2$. In each case a dashed line indicates the energy $2E_{J,\mathrm{T}}$, maximum potential energy.

should therefore be permissible to replace the ring to which the particle is confined with the whole real line, and the cosine potential with a parabola. Note that this approximation ignores the restriction (S14), responsible for charge quantization. For states with energies $\ll E_{J,\mathrm{T}}$, the phase is confined very close to the minimum at $\varphi = 0$ of the cosine potential, and the replacement $E_{J,\mathrm{T}}(1-\cos\widehat{\varphi}_0) \to E_{J,\mathrm{T}}\,\widehat{\varphi}_0^2\,/2$ is legitimate. This leads to a harmonic spectrum $\omega_n = \sqrt{E_{C,\mathrm{T}}E_{J,\mathrm{T}}}(n+1/2)$. However, the quadratic approximation can be improved to have a larger regime of validity, in the following way. We approximate the eigenstates of the **isolated** transmon as those of the parent Hamiltonian

$$H_P = \frac{E_{C,\mathrm{T}}}{2}\,\widehat{\mathrm{n}}_{\mathrm{T}}^2 + \frac{E_S}{2}\,\widehat{\varphi}_{\mathrm{T}}^2, \tag{S18}$$

where the parameter E_S is optimized according to some criterium in order to give the best possible agreement with the exact solution. Here we use the criterion that the energy E_S should be chosen to minimize $\langle H_{\mathrm{T}}\rangle$ where the expectation value is taken with respect to the ground state of H_P. For given E_S, the eigenstates and energies of H_P are

$$|n\rangle = \frac{(B^\dagger)^n}{\sqrt{n!}}\,|0\rangle\,, \quad E_n^{(0)} = \omega_{\mathrm{T}}(n+1/2), \quad n = 0,\,1,\,2,\,\ldots, \quad \omega_{\mathrm{T}} = \sqrt{E_{C,\mathrm{T}}E_S}, \tag{S19}$$

where

$$B\,|0\rangle = 0, \quad B = \lambda\,\widehat{\mathrm{n}}_{\mathrm{T}} + i\,\widehat{\varphi}_{\mathrm{T}}\,/2\lambda, \quad \lambda = \frac{1}{\sqrt{2}}\left(\frac{E_{C,\mathrm{T}}}{E_S}\right)^{1/4}. \tag{S20}$$

Expressed in terms of the bosonic opertors B and $B^\dagger$, and manipulated into normal ordered form, the full transmon Hamiltonian reads

$$\begin{aligned} H_{\mathrm{T}} =& \omega_{\mathrm{T}}\left[B^\dagger B + \frac{1}{2}\right] + E_{J,\mathrm{T}}\left\{1 - \frac{e^{-\lambda^2/2}}{2}\left[e^{\lambda B^\dagger}e^{-\lambda B} + e^{-\lambda B^\dagger}e^{\lambda B}\right]\right\} \\ &+ \frac{E_S}{2}\lambda^2\left[(B^\dagger)^2 + B^2 - 2(B^\dagger B + 1)\right]. \end{aligned} \tag{S21}$$

The expectation value $\langle 0|\,H_{\mathrm{T}}\,|0\rangle$ evaluates to

$$\langle 0|\,H_{\mathrm{T}}\,|0\rangle = \frac{\omega_{\mathrm{T}}}{4} + E_{J,\mathrm{T}}\left(1 - e^{-\lambda^2/2}\right) = \frac{\sqrt{E_{C,\mathrm{T}}E_S}}{4} + E_{J,\mathrm{T}}\left[1 - e^{-\sqrt{E_{C,\mathrm{T}}/E_S}/4}\right]. \tag{S22}$$

The minimal value for $\langle 0|\,H_{\mathrm{T}}\,|0\rangle$ is produced by E_S satisfying the equation

$$E_S = E_{J,\mathrm{T}}e^{-\sqrt{E_{C,\mathrm{T}}/E_S}/4}, \tag{S23}$$

which can also be written as an equation

$$\omega_{\rm T} = \sqrt{E_{J,{\rm T}} E_{C,{\rm T}}} e^{-E_{C,{\rm T}}/8\omega_{\rm T}}, \tag{S24}$$

determining the transmon frequency $\omega_{\rm T}$. We note that in principle, the approximation can be further improved by treating H_P with the optimized value (S23) for E_S as the zero'th order approximation and treating $H_{\rm T} - H_P$ as a small perturbation. In general, the leading corrections in such a perturbation expansion are of first order in λ^2. However, for the ground and first excited states, it is one order higher, i.e. λ^4. Thus, the approximation $H_{\rm T} \simeq H_P$ is particularly accurate for the ground and first excited states of the transmon, which given the probe power and plasma frequency of the chain, are the ones we are interested in, in the experiment. The assumed smallness of λ allows us to

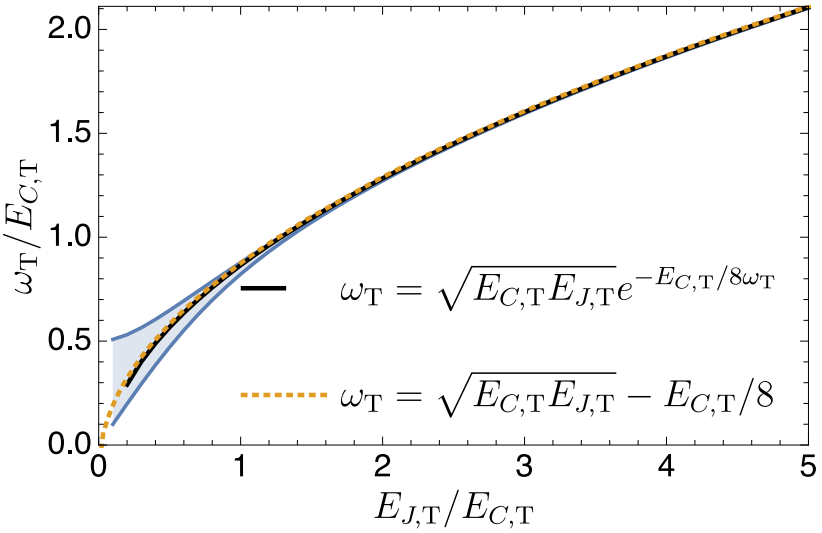

FIG. S11. **From the transmon to the Cooper pair box.** Excitation energy $\omega_{\rm T}$ from the ground state to the first excited state of the isolated transmon. The shaded area respresents the range of values obtained for the exact result when the offset charge $n_{\rm T}$ is swept through $[0, 1/2]$. The solid black line represents the fully self-consistent result (S24) while the dashed line represents the simple approximation (S26) .

solve approximately the self-consistency equation (S23) to get

$$E_S = E_{J,{\rm T}} - \frac{1}{4}\sqrt{E_{C,{\rm T}} E_{J,{\rm T}}} + \mathcal{O}\left(E_{C,{\rm T}}\right), \tag{S25}$$

which gives an excitation energy

$$\omega_{\rm T} = \sqrt{E_{C,{\rm T}} E_{J,{\rm T}}} - E_{C,{\rm T}}/8 + \mathcal{O}\left(\frac{E_{C,{\rm T}}^2}{\sqrt{E_{C,{\rm T}} E_{J,{\rm T}}}}\right). \tag{S26}$$

In Figure S11 we compare the results (S24) and (S26) to the exact excitation energy of the isolated transmon, and find that in the regime where sensitivity to the offset charge $n_{\rm T}$ is weak, i.e. $E_{J,{\rm T}}/E_{C,{\rm T}} \gtrsim 1$, the approximation (S26) is indistinguishable from the more sophisticated (S24). Now we turn to the case $E_J > 0$ where the transmon is coupled to the dynamical degrees of freedom in the chain. We take the same approach as before. In principle, it is possible to generalize the previous calculation in the following way. When $E_J > 0$, we may choose E_S so that it minimizes $\langle 0| H |0\rangle$, where H is the full Hamiltonian in (Eq. 4 in the main text)

$$H = \frac{(2e)^2}{2} \vec{\hat{\rm n}}^T \hat{\rm C}^{-1} \vec{\hat{\rm n}} - \frac{1}{2} \vec{\hat{\varphi}}^T \hat{\rm J} \vec{\hat{\varphi}} - E_{J,{\rm T}} \cos\left(\hat{\varphi}_R - \hat{\varphi}_L\right), \tag{S27}$$

and $|0\rangle$ is the ground state of the parent Hamiltonian that is obtained from H by making the replacement $E_{J,{\rm T}}(1 - \cos\hat{\varphi}_{\rm T}) \to E_S\,\hat{\varphi}_{\rm T}^2/2$. We have implemented this approach, but find that it yields an insignificant improvement upon the simpler approach of simply taking $E_S = E_{J,{\rm T}} - \sqrt{E_{J,{\rm T}} E_{C,{\rm T}}}/4$, at least in the one photon sector, and for the parameters of the current device.

G. Analytical formula for the Scattering Phase Shift

In the section *Methods - Analytical formula for the Scattering Phase Shift* we presented a formula (Eq. 11) for the phase shift $\phi(\omega, \Phi_{\rm T}, \Phi_{\rm C})$ of a mode with frequency ω of the full system at transmon flux $\Phi_{\rm T}$ and chain flux $\Phi_{\rm C}$:

$$\tan\phi(\omega,\Phi_{\rm T},\Phi_{\rm C}) = \frac{C_{\rm g}-2C_{\rm eff}(\Phi_{\rm T},\omega)}{\sqrt{C_{\rm g}(C_{\rm g}+4C_J)}}\frac{1}{\sqrt{\left(\frac{\omega_{\rm p}(\Phi_{\rm C})}{\omega}\right)^2-1}}. \tag{S28}$$

Here we give the derivation. We work in the thermodynamic limit where $N\to\infty$. This means that both matrices $\widehat{\rm C}$ and $\widehat{\rm J}$ (Eqs. (S32) and (S33)) become semi-infinite. Furthermore, the approximation discussed in the previous section eliminates the anharmonic term in H, and introduces four new non-zero matrix elements in $\widehat{\rm J}$, namely

$$\widehat{\rm J}_{L,L} = \widehat{\rm J}_{R,R} = E_S\left(\Phi_{\rm T}\right), \tag{S29}$$

$$\widehat{\rm J}_{R,L} = \widehat{\rm J}_{L,R} = -E_S\left(\Phi_{\rm T}\right). \tag{S30}$$

Making the flux-dependence of E_S explicit, we have from Eq. (S25)

$$E_S\left(\Phi_{\rm T}\right) = E_{J,{\rm T}}\left(\Phi_{\rm T}\right) - \sqrt{E_{J,{\rm T}}\left(\Phi_{\rm T}\right)E_{C,{\rm T}}}/4, \tag{S31}$$

with $E_{J,{\rm T}}\left(\Phi_{\rm T}\right) = E_{J,T,\max}\left|\cos\left(\pi\Phi_{\rm T}/\Phi_0\right)\right|$. Explicitly the matrices $\widehat{\rm C}$ and $\widehat{\rm J}$ then read (see Eqs. (6) and (7) in the main text)

$$\widehat{\rm C} = \begin{pmatrix} C_0 & -C_{\rm sh,T} & 0 & 0 & 0 & 0 & \cdots \\ -C_{\rm sh,T} & C_0 & -C_{\rm c} & 0 & 0 & 0 & \cdots \\ 0 & -C_{\rm c} & C_1 & -C_J & 0 & 0 & \cdots \\ 0 & 0 & -C_J & C_\Sigma & -C_J & 0 & \cdots \\ \vdots & \vdots & \vdots & \ddots & \ddots & \ddots & \ldots \end{pmatrix} \tag{S32}$$

$$\widehat{\rm J} = \frac{\varphi_0^2}{L_J\left(\Phi_{\rm C}\right)}\begin{pmatrix} 0&0&0&0&0&0&\cdots\\ 0&0&0&0&0&0&\cdots\\ 0&0&1&-1&0&0&\cdots\\ 0&0&-1&2&-1&0&\cdots\\ \vdots&\vdots&\vdots&\ddots&\ddots&\ddots&\ldots \end{pmatrix} + E_S(\Phi_{\rm T})\begin{pmatrix} 1&-1&0&0&0&0&\cdots\\ -1&1&0&0&0&0&\cdots\\ 0&0&0&0&0&0&\cdots\\ 0&0&0&0&0&0&\cdots\\ \vdots&\vdots&\vdots&\vdots&\vdots&\vdots&\ddots \end{pmatrix} \tag{S33}$$

We now have a fully linear system. The phase shifts in Eq. (S28) are obtained by solving the classical equations of motion. We start by defining a vector with the superconducting phases in each island $\vec{\pi}^T = (\varphi_L, \varphi_R, \varphi_1, \varphi_2, \cdots, \varphi_N)$. The equations of motion for the mode at frequency ω are given by

$$\widehat{\rm J}\left(\Phi_{\rm T},\Phi_{\rm C}\right)\vec{\pi}_\omega = (\hbar\omega)^2\frac{\widehat{\rm C}}{(2e)^2}\vec{\pi}_\omega. \tag{S34}$$

The solution to the part of Eq. (S34) involving degrees of freedom in the chain can be taken as

$$\varphi_j = N(\omega)\cos\left[j\kappa(\omega,\Phi_{\rm C})a - \phi(\omega,\Phi_{\rm T},\Phi_{\rm C})\right] \quad \text{with} \quad j = 1,2,3,4\ldots \tag{S35}$$

Here a is the length of the unit cell of the array, $N(\omega)$ a frequency dependent amplitude and $\kappa(\omega,\Phi_{\rm C})$ is the wave number of a wave that propagates in the chain with angular frequency ω. It can be obtained from the dispersion relation in Eq. (S2),

$$\kappa(\omega,\Phi_{\rm C}) = \frac{2}{a}\,\mathrm{arccot}\sqrt{\left(\frac{4C_J}{C_{\rm g}}+1\right)\left[\left(\frac{\omega_{\rm p}(\Phi_{\rm C})}{\omega}\right)^2-1\right]}, \tag{S36}$$

where $\omega_{\rm p}(\Phi_{\rm C}) = 1/\sqrt{L_J(\Phi_{\rm C})\left(C_J + C_{\rm g}/4\right)}$ is the plasma frequency of the chain. The phase shift $\phi(\omega,\Phi_{\rm T},\Phi_{\rm C})$ in Eq. (S35) is determined by the components of Eq. (S34) involving the transmon islands. They read

$$E_S\left(\Phi_{\rm T}\right)\left(\varphi_L-\varphi_R\right) = \frac{(\hbar\omega)^2}{(2e)^2}\left(C_0\varphi_L - C_{\rm sh,T}\varphi_R\right), \tag{S37}$$

$$E_S\left(\Phi_{\rm T}\right)\left(\varphi_R-\varphi_L\right) = \frac{(\hbar\omega)^2}{(2e)^2}\left(-C_{\rm sh,T}\varphi_L - C_0\varphi_R - C_{\rm c}\varphi_1\right), \tag{S38}$$

$$E_S\left(\Phi_{\rm T}\right)\left(\varphi_1-\varphi_2\right) = \frac{(\hbar\omega)^2}{(2e)^2}\left(-C_{\rm sh,T}\varphi_R - C_1\varphi_1 - C_J\varphi_2\right). \tag{S39}$$

Using Eq. (S37) and Eq. (S38) we eliminate φ_L and solve for φ_R in terms of φ_1 to obtain

$$\varphi_R = \frac{C_\mathrm{c}\left[\frac{(\hbar\omega)^2}{(2e)^2}C_0 - E_S(\Phi_\mathrm{T})\right]}{(C_0 - C_{\mathrm{sh,T}})\left[(C_0 + C_{\mathrm{sh,T}})\frac{(\hbar\omega)^2}{(2e)^2}C_0 - 2E_S(\Phi_\mathrm{T})\right]}\varphi_1. \tag{S40}$$

Substituting this into Eq. (S39) and using Eq. (S36) for $\kappa(\omega, \Phi_\mathrm{C})$ we obtain

$$\frac{C_\mathrm{g}}{2\left[1 - \cos\kappa(\omega, \Phi_\mathrm{C})a\right]}(\varphi_1 - \varphi_2) = C_{\mathrm{eff}}(\Phi_\mathrm{T}, \omega)\varphi_1, \tag{S41}$$

with

$$C_{\mathrm{eff}}(\Phi_\mathrm{T}, \omega) = C_1 - C_J - \frac{C_\mathrm{c}^2\left[\frac{(\hbar\omega)^2}{(2e)^2}C_0 - E_S(\Phi_\mathrm{T})\right]}{(C_0 - C_{\mathrm{sh,T}})\left[(C_0 + C_{\mathrm{sh,T}})\frac{(\hbar\omega)^2}{(2e)^2}C_0 - 2E_S(\Phi_\mathrm{T})\right]}. \tag{S42}$$

Using the mode definition in Eq. (S35) for φ_1 and φ_2 in Eq. (S41) leads to

$$\tan\phi(\omega, \Phi_\mathrm{T}, \Phi_\mathrm{C}) = \left[1 - \frac{2C_{\mathrm{eff}}(\Phi_\mathrm{T}, \omega)}{C_\mathrm{g}}\right]\tan\frac{\kappa(\omega, \Phi_\mathrm{C})a}{2}. \tag{S43}$$

Finally, using again the expression in Eq. (S36) for $\kappa(\omega, \Phi_\mathrm{C})$ we obtain the expression for the phase shift ϕ as a function of the system parameters.

$$\tan\phi(\omega, \Phi_\mathrm{T}, \Phi_\mathrm{C}) = \left[1 - \frac{2C_{\mathrm{eff}}(\Phi_\mathrm{T}, \omega)}{C_\mathrm{g}}\right]\sqrt{\frac{C_\mathrm{g}}{C_\mathrm{g} + 4C_J}}\frac{1}{\sqrt{\left(\frac{\omega_\mathrm{p}(\Phi_\mathrm{C})}{\omega}\right)^2 - 1}}. \tag{S44}$$

H. Link between the scattering phase shift and the relative frequency shift

In the main text we defined the relative frequency shift $\delta\phi_n$ in terms of the discrete mode frequencies of the full system (transmon plus finite chain of N nodes) at respective transmon fluxes Φ_T and $\Phi_0/2$. We repeat the definition here:

$$\delta\phi_n(\Phi_\mathrm{T}, \Phi_\mathrm{C}) = \pi\frac{\omega_n(\Phi_0/2, \Phi_\mathrm{C}) - \omega_n(\Phi_\mathrm{T}, \Phi_\mathrm{C})}{\omega_n(\Phi_0/2, \Phi_\mathrm{C}) - \omega_{n-1}(\Phi_0/2, \Phi_\mathrm{C})}. \tag{S45}$$

Here we relate this to the relative scattering phase shift $\delta\phi(\omega, \Phi_\mathrm{T}, \Phi_\mathrm{C})$ for the infinite system (see Eq. 14 in the *Methods* section of the main text) by showing that

$$\delta\phi_n(\Phi_\mathrm{T}, \Phi_\mathrm{C}) = \delta\phi(\omega_n(\Phi_\mathrm{T}, \Phi_\mathrm{C}), \Phi_\mathrm{T}, \Phi_\mathrm{C}) + \mathcal{O}(N^{-1}). \tag{S46}$$

For conveniece we assume that island $N+1$ is grounded. (The precise boundary condition becomes immaterial in the $N \to \infty$ limit.) Had the chain been open to the left of node 1, the eigenmodes would have been $\varphi_j \propto \cos\left(\kappa_n^0 aj\right)$, $j \in 1, 2, 3, \ldots, N$ with wave numbers given by $\kappa_n^0 = (n - 1/2)\pi/Na$ with $n \in 1, 2, 3, \ldots, N$. In the presence of the transmon to the left of chain node 1, the eigenmodes inside the chain change to $\cos\left(\kappa_n aj - \phi_n\right)$. Here ϕ_n is the additional phase introduced by the transmon. Now the κ_n depend on ϕ_n too. Assuming the boundary conditions that the nodes to the left of transmon island L and to the right of chain island N are grounded, they are given by

$$\kappa_n a = \frac{\left(n - \frac{1}{2}\right)\pi}{N} + \frac{\phi_n}{N} = \kappa_n^0 a + \frac{\phi_n}{N}. \tag{S47}$$

The modes of the system follow a dispersion relation $\omega_n\left(\Phi_\mathrm{T}, \Phi_\mathrm{C}\right) = \omega(\Phi_\mathrm{C}, \kappa_n)$. The notation must be understood as follows: $\omega_n(x, y)$ and $\omega(x, y)$ denote distinct functions. The two arguments of the former refer to respectively the flux in a transmon and in a chain SQUID, and for given fluxes, the function assumes the value of the frequency of system mode n. The first argument of the latter function $\omega(x, y)$ refers to the flux in a chain SQUID, while the second argument refers to the unquantized wave number of a mode in the infinite chain. The function evaluates to

the frequency corresponding to the given wave number (which does not depend on the transmon flux). For sufficiently large N we can expand the dispersion relation around $\kappa_n^0 a$

$$\omega_n\left(\Phi_{\mathrm{T}},\Phi_{\mathrm{C}}\right)=\omega\left(\Phi_{\mathrm{C}},\kappa_n^0\right)+\frac{\phi_n\left(\Phi_{\mathrm{T}},\Phi_{\mathrm{C}}\right)}{N}\left.\frac{\partial\omega(\Phi_{\mathrm{C}},\kappa)}{\partial\left(\kappa a\right)}\right|_{\kappa=\kappa_n^0}, \tag{S48}$$

with corrections of order N^{-2}. The dependence on the transmon and chain fluxes is included. Similarly, we can expand $\omega_{n-1}\left(\Phi_{\mathrm{T}},\Phi_{\mathrm{C}}\right)$ around $\kappa_n^0 a$ to obtain

$$\omega_{n-1}\left(\Phi_{\mathrm{T}},\Phi_{\mathrm{C}}\right)=\omega_n\left(\Phi_{\mathrm{T}},\Phi_{\mathrm{C}}\right)-\frac{\pi}{N}\left.\frac{\partial\omega(\Phi_{\mathrm{C}},\kappa)}{\partial\left(\kappa a\right)}\right|_{\kappa=\kappa_n^0}. \tag{S49}$$

Here we made use of the fact that $\phi_n-\phi_{n-1}=\mathcal{O}\left(N^{-1}\right)$. Therefore we can set $\phi_{n-1}=\phi_n$ introducing an error of $\mathcal{O}\left(N^{-2}\right)$ which can be ignored for large N. We can now obtain the terms in Eq. (S45),

$$\omega_n\left(\Phi_0/2,\Phi_{\mathrm{C}}\right)=\omega\left(\Phi_{\mathrm{C}},\kappa_n^0\right)+\frac{\phi_n\left(\Phi_0/2,\Phi_{\mathrm{C}}\right)}{N}\left.\frac{\partial\omega(\Phi_{\mathrm{C}},\kappa)}{\partial\left(\kappa a\right)}\right|_{\kappa=\kappa_n^0} \tag{S50}$$

$$\omega_n\left(\Phi_{\mathrm{T}},\Phi_{\mathrm{C}}\right)=\omega\left(\Phi_{\mathrm{C}},\kappa_n^0\right)+\frac{\phi_n\left(\Phi_{\mathrm{T}},\Phi_{\mathrm{C}}\right)}{N}\left.\frac{\partial\omega(\Phi_{\mathrm{C}},\kappa)}{\partial\left(\kappa a\right)}\right|_{\kappa=\kappa_n^0} \tag{S51}$$

$$\omega_{n-1}\left(\Phi_0/2,\Phi_{\mathrm{C}}\right)=\omega_n\left(\Phi_0/2,\Phi_{\mathrm{C}}\right)-\frac{\pi}{N}\left.\frac{\partial\omega(\Phi_{\mathrm{C}},\kappa)}{\partial\left(\kappa a\right)}\right|_{\kappa=\kappa_n^0}. \tag{S52}$$

Substituting this into Eq. (S45), and noting that $\phi_n\left(\Phi_{\mathrm{T}},\Phi_{\mathrm{C}}\right)=\phi\left(\omega_n(\Phi_{\mathrm{T}},\Phi_{\mathrm{C}}),\Phi_{\mathrm{T}},\Phi_{\mathrm{C}}\right)$, we obtain Eq. (S46).

I. Relation between the Phase Shift and the impurity response function

To elaborate the link between the local impurity response function and the phase shift induced by the transmon qubit, we define three spectral densities

$$A_1(\omega)=\frac{2E_S(\Phi_{\mathrm{T}})}{\omega_{\mathrm{T}}}\mathrm{Re}\int_0^\infty\frac{dt}{2\pi}e^{i\omega t}\left\langle[\widehat{\varphi}_{\mathrm{T}}(t),\widehat{\varphi}_{\mathrm{T}}(0)]\right\rangle, \tag{S53}$$

$$A_2(\omega)=-\mathrm{Im}\int_0^\infty\frac{dt}{2\pi}e^{i\omega t}\left\langle[\widehat{\varphi}_{\mathrm{T}}(t),\widehat{\mathrm{n}}_{\mathrm{T}}(0)]\right\rangle, \tag{S54}$$

$$A_3(\omega)=\frac{2\omega_{\mathrm{T}}}{E_S(\Phi_{\mathrm{T}})}\mathrm{Re}\int_0^\infty\frac{dt}{2\pi}e^{i\omega t}\left\langle[\widehat{\mathrm{n}}_{\mathrm{T}}(t),\widehat{\mathrm{n}}_{\mathrm{T}}(0)]\right\rangle, \tag{S55}$$

corresponding to the phase-phase, phase-charge and charge-charge response of the transmon up to constant prefactors. In order to calculate these spectral densities we turn to the quantum mechanical problem (In the previous section, we could compute the phase shift by solving the classical equations of motion). With each mode ω we associate cannonical bosonic operators b_ω and $b_\omega^\dagger$. These are related to the charge operator $\widehat{\mathrm{n}}_j$ and phase operator $\widehat{\varphi}_j$ for each of the islands as

$$\widehat{\varphi}_j=\frac{-i}{\sqrt{2}}\int_0^{\omega_{\mathrm{p}}(\Phi_{\mathrm{C}})}d\omega\varphi_j(\omega)\left(b_\omega-b_\omega^\dagger\right), \tag{S56}$$

$$\widehat{\mathrm{n}}_j=\frac{1}{\sqrt{2}}\int_0^{\omega_{\mathrm{p}}(\Phi_{\mathrm{C}})}\frac{d\omega}{\omega}\sum_{l=L,R,1,2,\cdots}\widehat{\mathrm{J}}(\Phi_{\mathrm{T}},\Phi_{\mathrm{C}})_{j,l}\varphi_l(\omega)\left(b_\omega+b_\omega^\dagger\right), \tag{S57}$$

where the profile $\varphi_j(\omega)$ is normalized such that

$$\sum_{j=L,R,1,2,\cdots}\varphi_j(\omega)\,\widehat{\mathrm{J}}(\Phi_{\mathrm{T}},\Phi_{\mathrm{C}})_{j,l}\varphi_l(\omega')=\omega\delta(\omega-\omega'). \tag{S58}$$

The normalization constant in Eq. (S35) is thus set to

$$N_\omega=\sqrt{\frac{\hbar\omega}{\pi E_J(\Phi_{\mathrm{C}})[1-\cos\kappa(\omega,\Phi_{\mathrm{C}})]}\frac{\partial\kappa(\omega,\Phi_{\mathrm{C}})}{\partial\omega}}. \tag{S59}$$

From the definition of $\hat{\mathrm{n}}_\mathrm{T}$ and $\hat{\varphi}_\mathrm{T}$ (see the text below Eq. 7 in the *Methods* section of the main text) follows

$$\hat{\mathrm{n}}_\mathrm{T} = (\hat{\mathrm{n}}_R - \hat{\mathrm{n}}_L)/2 = \frac{1}{\sqrt{2}} \int_0^{\omega_\mathrm{p}(\Phi_\mathrm{C})} d\omega \frac{E_S(\Phi_\mathrm{C})}{\omega} \left[\varphi_R(\omega) - \varphi_L(\omega)\right] \left(b_\omega + b_\omega^\dagger\right), \tag{S60}$$

$$\hat{\varphi}_\mathrm{T} = \hat{\varphi}_R - \hat{\varphi}_L = \frac{-i}{\sqrt{2}} \int_0^{\omega_\mathrm{p}(\Phi_\mathrm{C})} d\omega \left[\varphi_R(\omega) - \varphi_L(\omega)\right] \left(b_\omega - b_\omega^\dagger\right). \tag{S61}$$

Explicitly, we find:

$$\varphi_R(\omega) - \varphi_L(\omega) = N_\omega \frac{C_\mathrm{c}\omega^2/(2e)^2}{(C_0 + C_{\mathrm{sh,T}})\omega^2/(2e)^2 - 2E_S(\Phi_\mathrm{T})} \cos\phi(\omega, \Phi_\mathrm{T}, \Phi_\mathrm{C}). \tag{S62}$$

In the Heisenberg picture $b_\omega(t) = e^{i\omega t} b_\omega$ and $b_\omega^\dagger(t) = e^{-i\omega t} b_\omega^\dagger$. Using this to calculate the spectral densities $A_j(\omega)$ for $\omega > 0$ we obtain

$$A_1(\omega) = \frac{E_S(\Phi_\mathrm{T})}{\omega_\mathrm{T}} \left[\varphi_R(\omega) - \varphi_L(\omega)\right]^2, \tag{S63}$$

$$A_2(\omega) = \frac{E_S(\Phi_\mathrm{T})}{\omega} \left[\varphi_R(\omega) - \varphi_L(\omega)\right]^2, \tag{S64}$$

$$A_3(\omega) = \frac{E_S(\Phi_\mathrm{T})\omega_\mathrm{T}}{\omega^2} \left[\varphi_R(\omega) - \varphi_L(\omega)\right]^2 \tag{S65}$$

Now we compare the three correlation functions with the frequency derivative of $\delta\phi(\omega, \Phi_\mathrm{T}, \Phi_\mathrm{C}) = \phi(\omega, \Phi_\mathrm{T}, \Phi_\mathrm{C}) - \phi(\omega, \Phi_0/2, \Phi_\mathrm{C})$ with $\phi(\omega, \Phi_\mathrm{T}, \Phi_\mathrm{C})$ given in Eq. (S28). In Fig. S12 we plot the four curves. We see that the four curves overlap around the transmon frequency ω_T. This means that the width and the center frequency obtained from the scattering phase shift are good estimations of the real width Γ_T and frequency ω_T of the transmon.

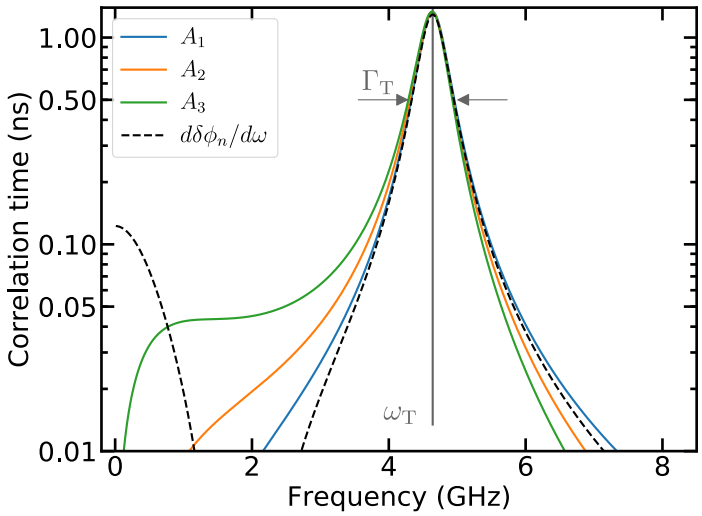

FIG. S12. **Connection between phase shifts and qubit dissipation.** Comparison between the three correlation functions and the energy derivative of the phase shift.

J. Breakdown of the rotating wave approximation

In this section, we investigate the applicability of the rotating wave approximation (RWA), a common technique for analysing the light-matter interaction at sufficiently weak coupling. The regime in which the light-matter coupling is so large that this approximation becomes inaccurate, is referred to as ultra-strong coupling. We will find that indeed, the RWA leads to errors of a few percent for our device.

To set up the RWA, we have to identify the harmonic oscillator basis that diagonalizes the (finite) chain part of the Hamiltonain. For this purpose, it is convenient to define $N \times N$ matrices $\widehat{C}^{-1}_{\rm chain}$ and $\widehat{L}^{-1}_{\rm chain}$ with entries

$$[\widehat{C}^{-1}_{\rm chain}]_{jk} = [\widehat{C}^{-1}]_{jk}, \quad [\widehat{L}^{-1}_{\rm chain}]_{jk} = [\widehat{J}]_{jk}/\varphi_0^2, \quad j,\, k = 1,\, 2,\, \ldots,\, N, \tag{S66}$$

i.e. $\widehat{C}^{-1}_{\rm chain}$ and $\varphi_0^2\widehat{L}^{-1}_{\rm chain}$ are the lower right $N \times N$ blocks of respectively the inverse of the full $(N+2) \times (N+2)$ capacitance matrix $\widehat{C}$, and of the full $(N+2) \times (N+2)$ Josephson matrix $\widehat{J}$. We then define an $N \times N$ matrix $\widehat{\Pi}_{\rm chain}$ and a positive definite diagonal matrix $\widehat{\omega}_{\rm chain}$ such that the columns of $\widehat{\Pi}_{\rm chain}$ contain the eigenvectors of $\widehat{C}^{-1}_{\rm chain}\widehat{L}^{-1}_{\rm chain}$ while the diagonal entries of $(\widehat{\omega}_{\rm chain})^2$ are the corresponding eigenvalues, i.e.

$$\widehat{C}^{-1}_{\rm chain}\widehat{L}^{-1}_{\rm chain}\widehat{\Pi}_{\rm chain} = \widehat{\Pi}_{\rm chain}(\widehat{\omega}_{\rm chain})^2. \tag{S67}$$

Since the eigenvalues are real, we can and will choose the entries of $\widehat{\Pi}_{\rm chain}$ to be real as well. This definition determines each column of $\widehat{\Pi}_{\rm chain}$ up to a normalization constant. We fix these constants by demanding that

$$\varphi_0^2 \sum_{jk} [\widehat{L}^{-1}_{\rm chain}]_{jk}[\widehat{\Pi}_{\rm chain}]_{jl}[\widehat{\Pi}_{\rm chain}]_{kl} = \hbar[\omega_{\rm chain}]_l, \tag{S68}$$

where $[\omega_{\rm chain}]_l$ is the l'th diagonal entry of $\widehat{\omega}_{\rm chain}$. We also define a matrix

$$\widehat{\Xi}_{\rm chain} = \varphi_0^2\widehat{L}^{-1}_{\rm chain}\widehat{\Pi}_{\rm chain}\widehat{\omega}^{-1}_{\rm chain}/\hbar. \tag{S69}$$

It is easy to verify that the row l of $\widehat{\Xi}^{\rm T}_{\rm chain}$ contains the left-eigenvector of $\widehat{C}^{-1}_{\rm chain}\widehat{L}^{-1}_{\rm chain}$ that is associated with eigenvector $([\omega_{\rm chain}]_l)^2$. As a result $\widehat{\Xi}^{\rm T}_{\rm chain}\widehat{\Pi}_{\rm chain}$ is guaranteed to be a diagonal matrix. Furthermore, due to the normalization condition (S68) we chose for $\widehat{\Pi}_{\rm chain}$, the diagonal entries of $\widehat{\Xi}^{\rm T}_{\rm chain}\widehat{\Pi}_{\rm chain}$ are all equal to unity. Thus

$$\widehat{\Xi}^{\rm T}_{\rm chain} = \widehat{\Pi}^{-1}_{\rm chain}. \tag{S70}$$

We now define N operators

$$\widehat{b}_{{\rm chain},k} = \frac{1}{\sqrt{2}} \sum_{j=1}^{N} \left\{ \widehat{n}_j[\widehat{\Pi}_{\rm chain}]_{jk} + i\widehat{\varphi}_j[\widehat{\Xi}_{\rm chain}]_{jk} \right\}. \tag{S71}$$

Owing to (S70) and the fact that $[\widehat{n}_j, \widehat{\varphi}_k] = i\delta_{j,k}$, the operators $\widehat{b}_{{\rm chain},k}$, $k = 1,\, 2,\, \ldots,\, N$ are bosonic annihilation operators, i.e. $[\widehat{b}_{{\rm chain},j}, \widehat{b}_{{\rm chain},k}] = 0$ and $[\widehat{b}_{{\rm chain},j}, \widehat{b}^\dagger_{{\rm chain},k}] = \delta_{j,k}$. Furthermore, for the chain part of the Hamiltonian we obtain

$$\begin{aligned} H_{\rm chain} &= \frac{1}{2} \sum_{j,k=1}^{N} \left\{ (2e)^2 [\widehat{C}^{-1}_{\rm chain}]_{jk}\widehat{n}_j\widehat{n}_k + \varphi_0^2[\widehat{L}^{-1}_{\rm chain}]_{jk}\widehat{\varphi}_k\widehat{\varphi}_j \right\} \\ &= \hbar \sum_{j=1}^{N} [\omega_{\rm chain}]_j \left(\widehat{b}^\dagger_{{\rm chain},j}\widehat{b}_{{\rm chain},j} - \frac{1}{2} \right). \end{aligned} \tag{S72}$$

For the term in the Hamiltonian that couples the transmon to the chain, we find

$$\begin{aligned} H_{\rm coupling} &= \widehat{n}_{\rm T} \sum_{j=1}^{N} \nu_j \widehat{n}_j \\ &= \frac{1}{\sqrt{2}} \widehat{n}_{\rm T} \sum_{k=1}^{N} g_k \left(\widehat{b}_{{\rm chain},k} + \widehat{b}^\dagger_{{\rm chain},k} \right) \end{aligned} \tag{S73}$$

where

$$g_k = \sum_{j=1}^{N} \nu_j [\widehat{\Xi}_{\rm chain}]_{jk}. \tag{S74}$$

A standard way to proceed from here is to truncate the full Hilbert space of the transmon to the subspace spanned by two lowest energy eigenstates $|0_{\rm T}\rangle$ and $|1_{\rm T}\rangle$ of the isolated transmon Hamiltonian (S13). This leads to a Hamiltonian of the Jaynes-Cummings type, ubiquitous in Quantum Optics. At sufficiently weak coupling, the expectation is that this should be accurate for studying the situation where a near-resonant excitation from the chain induces a transition between the ground and first excited states of the transmon. The operator $\widehat{n}_{\rm T}$ is replaced by

$$\widehat{n}_{\rm T} \simeq \langle 0_{\rm T}|\,\widehat{n}_{\rm T}\,|1_{\rm T}\rangle\,\{|0_{\rm T}\rangle\langle 1_{\rm T}| + |1_{\rm T}\rangle\langle 0_{\rm T}|\}\,, \tag{S75}$$

where we've chosen the overall phases of $|0_{\rm T}\rangle$ and $|1_{\rm T}\rangle$ such that $\langle 0_{\rm T}|\,\widehat{n}_{\rm T}\,|1_{\rm T}\rangle$ is real.

Alternatively, a more controlled way to proceed is to make the self-consistent harmonic approximation (SCHA) (see Sec. F), which we have shown to be well-justified, and to express $\widehat{n}_{\rm T}$ in terms of the resulting bosonic transmon operators [see Eq. (S20)], i.e.

$$\widehat{n}_{\rm T} = \frac{1}{\sqrt{2}}\left(\frac{E_{\rm C,T}}{E_{\rm S}}\right)^{1/4}(B + B^\dagger). \tag{S76}$$

After the SCHA, the Hamiltonian becomes quadratic, and no further approximations are required. We will however still consider the effect of making the RWA on this quadratic Hamiltonian, in order to asses whether or not the assumptions underpinning the RWA are valid in our device.

The RWA approximation now involves dropping the transmon-chain coupling terms in which the transmon (in the unperturbed basis) is excited while a boson is emitted into the chain, or the transmon is de-exited while a boson is absorbed from the chain. We adopt the standard nomenclature and refer to the dropped terms as "counter-rotating" (based on their time-dependence in the Dirac picture). Depending on whether this approximation is made in conjunction with truncating the transmon Hilbert space or with the SCHA, we either obtain an RWA Hamiltonian

$$\begin{aligned} H_{\rm RWA,1} = {} & (E_{1,\rm T} - E_{0,\rm T})\,|1_{\rm T}\rangle\langle 1_{\rm T}| + \sum_{n=1}^{N}\hbar[\omega_{\rm chain}]_n\widehat{b}^\dagger_{{\rm chain},n}\widehat{b}_{{\rm chain},n} \\ & + \frac{1}{\sqrt{2}}\langle 0_{\rm T}|\,\widehat{n}_{\rm T}\,|1_{\rm T}\rangle\sum_{k=1}^{N} g_k\left(|0_{\rm T}\rangle\langle 1_{\rm T}|\,\widehat{b}_{{\rm chain},k} + |1_{\rm T}\rangle\langle 0_{\rm T}|\,\widehat{b}^\dagger_{{\rm chain},k}\right), \end{aligned} \tag{S77}$$

or

$$H_{\rm RWA,2} = \omega_{\rm T}B^\dagger B + \sum_{n=1}^{N}\hbar[\omega_{\rm chain}]_n\widehat{b}^\dagger_{{\rm chain},n}\widehat{b}_{{\rm chain},n} + \frac{1}{2}\left(\frac{E_{\rm C,T}}{E_{\rm S}}\right)^{1/4}\sum_{k=1}^{N} g_k\left(B^\dagger\widehat{b}_{{\rm chain},k} + \widehat{b}^\dagger_{{\rm chain},k}B\right). \tag{S78}$$

For both Hamiltonians, the ground state is trivial: the transmon is in its unperturbed ground state, and there are no bosonic excitations in the chain. We measure energy relative to this ground state. Both Hamiltonians leave invariant the subspace spanned by states in which there are no bosons in the chain, while the transmon is in its unperturbed first excited state, or there is one boson in the chain while the transmon is in its unperturbed ground state. The excited states relevant for spectroscopy at low driving power are found by diagonalizing the RWA Hamiltonians in this subspace.

In Figure S13 we compare the relative frequency shift (Eq. 1 in the main text) predicted by $H_{\rm RWA,1}$ and $H_{\rm RWA,2}$ to the analytical SCHA formula (Eq. 14 in the main text) derived for an infinite chain. We have also computed SCHA results for the finite chain of 4700 islands, and found that they lie on top of the infinite chain curves. We omit them from the figure to avoid clutter. We note that $H_{\rm RWA,1}$ and $H_{\rm RWA,2}$ give very similar results. This is consistent with our claim that at low energies, the SCHA Hamiltonian from which $H_{\rm RWA,2}$ derives, is a good approximation to the full Hamiltonian from which $H_{\rm RWA,1}$ is derived. We ascribe the small difference between results for $H_{\rm RWA,1}$ and $H_{\rm RWA,2}$ to the truncation by hand in $H_{\rm RWA,1}$ of the transmon Hilbert space to two states. (No such by-hand truncation was required in $H_{\rm RWA,2}$.) If we fit an arctan line shape (Eq. 18 in the main text) to the SCHA curves in the figure, we find that the transmon resonance occurs at a frequency within about 0.01 GHz from h^{-1} times the energy difference between the ground and first excited states of the isolated transmon. Using the same procedure on the relative frequency shift predicted by either $H_{\rm RWA,1}$ or $H_{\rm RWA,2}$ on the other hand, gives a resonance frequency that is ~ 0.1 GHz higher than h^{-1} times the ground to first excitation energy of the isolated transmon. We conclude that the RWA approximation is not quantitatively accurate, producing an error of between 2% and 5% for the transmon resonance frequency. This signals that our device indeed operates in the ultra-strong light-matter coupling regime.

[1] N. Masluk, I. Pop, A. Kamal, Z. Minev, and M. Devoret, Physical Review Letters **109**, 137002 (2012).

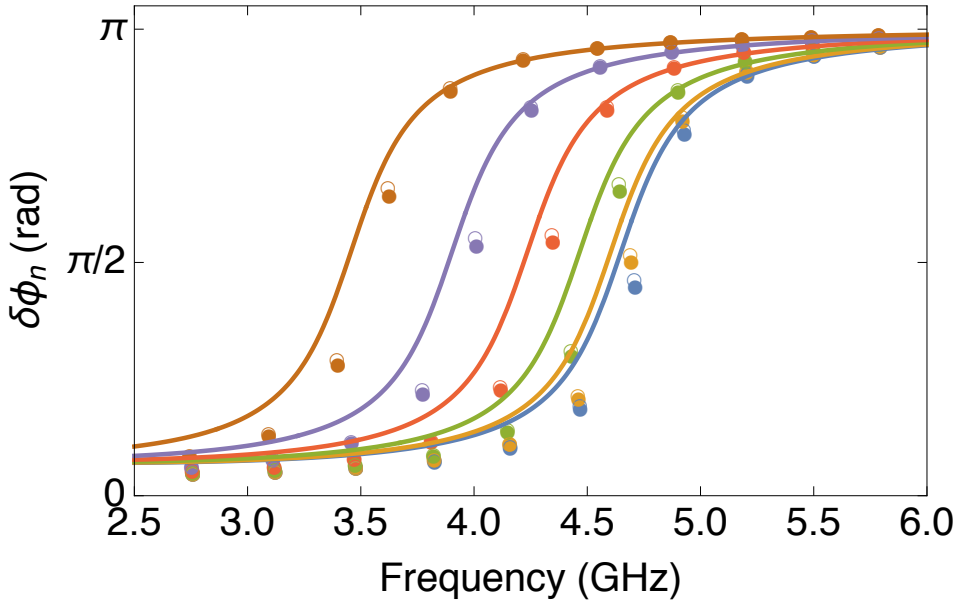

FIG. S13. **Deviations from the microscopic model under the RWA assumption.** Curves show the analytical formula for the relative frequency shift (Eq. 14 in the main text). Open circles show the corresponding result calculated using $H_{\mathrm{RWA},1}$ and closed circles the result calculated using $H_{\mathrm{RWA},2}$. In all cases the system parameters were taken as in Table 1 of the main text. The flux Φ_{C} through chain SQUIDS was held fixed at zero. Results for six different fluxes $\Phi_T \in [0, 0.3\Phi_0]$ through the transmon SQUID are shown.

[2] T. Weissl, Quantum phase and charge dynamics in Josephson junction chains, Ph.D. thesis, Université Joseph Fourier (2014).

[3] T. Weissl, B. Küng, E. Dumur, A. K. Feofanov, I. Matei, C. Naud, O. Buisson, F. W. J. Hekking, and W. Guichard, Physical Review B **92**, 104508 (2015).

[4] A. Fay, Couplage variable entre un qubit de charge et un qubit de phase, Ph.D. thesis, Université Joseph Fourier (2008).

[5] D. A. Frickey, IEEE Transactions on microwave theory and techniques **42** (1994).

[6] D. Pozar, Microwave Engineering, edited by J. Wiley and Sons (John Wiley and Sons, 2005).

[7] J. Koch, T. M. Yu, J. Gambetta, A. A. Houck, D. I. Schuster, J. Majer, A. Blais, M. H. Devoret, S. M. Girvin, and R. J. Schoelkopf, Physical Review A **76**, 042319 (2007).